scientific reports

Check for updates

OPEN

Leucine rich repeat containing 15 promotes triple-negative breast cancer proliferation and invasion via the ITGB1/FAK/PI3K signalling pathway

Xiao Wu[1,2], Yameng Liu[2], Yinxi Hu[3], Fang Su[2], Zishu Wang[2], Yongxia Chen[2] & Zhixiang Zhuang[1]✉

Leucine rich repeat containing 15 (LRRC15) is recognized for its intimate association with the extracellular matrix, where it modulates fibroblast function and shapes the immune landscape within the tumour microenvironment. The specific expression patterns and molecular contributions of LRRC15 in triple-negative breast cancer(TNBC) have not been fully elucidated. This study aimed to delineate the clinical relevance and biological implications of LRRC15 in TNBC, and to assess its potential as a novel therapeutic target for this disease. Our findings revealed robust overexpression of LRRC15 in TNBC tumour tissues and cell lines, which was inversely correlated with patient survival outcomes. Notably, the suppression of LRRC15 expression led to pronounced inhibition of TNBC cell proliferation, invasion, and migration both in vitro and in vivo. Mechanistically, we established that LRRC15 interacts with Integrin Beta 1(ITGB1), facilitating the phosphorylation of the T788/T789 residues on ITGB1 and recruiting focal adhesion kinase (FAK) to the site of integrin aggregation. This recruitment promotes the downstream phosphorylation of PI3K and AKT, suggesting that LRRC15 is a key activator of the ITGB1/FAK/PI3K signalling pathway. Collectively, our data indicate that LRRC15 is a critical promoter of TNBC cell proliferation and metastasis through the activation of this signalling pathway, identifying LRRC15 as a promising candidate for therapeutic intervention in TNBC.

Keywords LRRC15, TNBC, ITGB1/FAK/PI3K signalling pathway, Proliferation, Invasion

According to Global Cancer Statistics, breast cancer is the most common malignancy among women worldwide[1]. Triple-negative breast cancer (TNBC) accounts for approximately 15% of all breast cancer cases and is distinguished by a higher recurrence rate and a shorter overall survival span than other breast cancer subtypes[2]. TNBC is characterized by an early age of onset, elevated level of malignancy, and accelerated rate of tumour progression[3,4]. Unlike luminal breast cancers, which are responsive to endocrine therapies, and HER2-positive tumours that can be targeted with anti-HER2 agents, TNBC is characterized by the absence of estrogen receptor (ER), progesterone receptor (PR), and human epidermal growth factor receptor 2 (HER2) expression[5]. The molecular profile of TNBC renders standard endocrine therapies and HER2-targeted treatments ineffective for TNBC, thereby constraining limiting therapeutic options primarily to chemotherapy, surgery, and radiation[6,7]. This triple-negative phenotype renders TNBC refractory to both hormonal therapies and HER2-directed treatments, constituting a critical unmet clinical need. The aetiology of TNBC is intricate and involves a complex interplay of molecular mechanisms such as genetic mutations, epigenetic alterations, and the aberrant activation of signalling pathways[8,9]. There is an imperative need for further in-depth research to unravel the complexities of TNBC and to devise more effective treatment strategies.

Leucine rich repeat containing 15 (LRRC15), a member of the Leucine-rich repeat (LRRC) superfamily, is a type I transmembrane protein encoded on chromosome 3q29[10]. This protein is pivotal in cellular processes, predominantly through its involvement in protein–protein and protein–matrix[11,12]. Recent studies have revealed the antiviral properties of LRRC15, which not only inhibits adenovirus infection but also prevents entry of the

[1]Department of Oncology, the Second Affiliated Hospital of Soochow University, Suzhou, China. [2]Department of Medical Oncology, the First Affiliated Hospital of Bengbu Medical University, Bengbu, China. [3]Department of Oncology, the First Affiliated Hospital of Soochow University, Suzhou, China. ✉email: Wuxiao091417@163.com

SARS-CoV-2 virus by binding to the spike protein on the viral envelope[13]. Notably, LRRC15 is highly expressed in mesenchymal-derived tumour cells and a variety of solid tumours[14,15]. There is evidence suggesting that LRRC15 expression in the tumour stroma influences fibroblast activity and collagen deposition[16]. Furthermore, LRRC15-positive tumour-associated fibroblasts have been shown to play a significant role in modulating the TME[17]. These attributes may be intricately connected to tumorigenesis, suggesting the potential oncogenic nature of LRRC15. While the involvement of LRRC15 in various cancers has been documented, its precise function and underlying mechanisms in TNBC have yet to be fully elucidated.

In this study, we observed that LRRC15 is upregulated to varying degrees in TNBC tissues and cell lines. Notably, an increased expression level of LRRC15 in TNBC patients is significantly associated with a poor prognosis. We further observed that the attenuation of LRRC15 markedly impeded the proliferation, invasion, and migration of TNBC cells in both in vitro and in vivo models. Conversely, the overexpression of LRRC15 reversed these cellular behaviours . Our findings also underscore the mechanistic role of LRRC15 in modulating the ITGB1 signalling axis. LRRC15 was found to interact with ITGB1, facilitating its transition from an inactive to an active conformation. This activation event triggers the recruitment of FAK to integrin-rich complexes and prompts the phosphorylation of FAK at the Y397 residue. This phosphorylation event initiates a downstream signalling cascade, leading to the activation of PI3K, which is a key regulator that promotes TNBC cell proliferation, invasion, and migration.

Results

LRRC15 is overexpressed in TNBC and is associated with poor prognosis

Our comprehensive analysis utilizing the TCGA database revealed that LRRC15 is significantly differentially expressed across a spectrum of cancers. Notably, LRRC15 was markedly upregulated in TNBC, luminal subtype breast cancer, HER-2-positive breast cancer, and ovarian cancer, whereas it was significantly downregulated in thyroid and endometrial cancers ($P < 0.001$) (Fig. S1A). We conducted a detailed analysis of TNBC data from TCGA, and compared LRRC15 expression levels between TNBC tissues and their adjacent noncancer counterparts in both paired and unpaired samples. Our analysis revealed that LRRC15 expression was significantly higher in cancerous tissues than in adjacent tissues ($P < 0.001$) (Fig. 1 A, B). To further investigate the relationship between LRRC15 expression and disease progression in TNBC patients, we performed immunohistochemical staining on tissue samples from 100 TNBC patients and scored them using the immunoreactive score (IRS) method, categorizing samples into low-expression ($IRS \leq 4$) and high expression groups ($IRS \geq 6$). The results indicated that LRRC15 protein expression was predominantly localized to the cell membrane (Fig. 1D), with 68 cases in the low-expression group and 32 cases in the high-expression group (Fig. 1E). Kaplan-Meier survival analysis revealed that TNBC patients with high LRRC15 expression had significantly shorter progression-free survival (PFS) than did those with low LRRC15 expression ($P = 0.049$) (Fig. 1C). Western blot (WB) analysis of fresh TNBC tissue samples confirmed that LRRC15 expression was significantly elevated in cancer tissues compared with adjacent tissues (Fig. 1F). Furthermore, LRRC15 expression was also elevated in four TNBC cell lines BT-20, BT-549, MDA-MB-468, and MDA-MB-231, compared with the normal human mammary epithelial cell line HBL-100 (Fig. 1G). These observations suggest that LRRC15 may be highly expressed in TNBC and could play a pivotal role in its pathogenesis. Clinicopathological analysis revealed that high LRRC15 expression was positively correlated with lymph node metastasis, TNM stage, and elevated Ki67 expression. However, it was not significantly correlated with age, menopausal status, number of primary tumours, histological grade, P53 expression, or receipt of neoadjuvant chemotherapy (Table 1). Univariate Cox proportional hazards analysis indicated that lymph node metastasis (with vs. without; $P = 0.013$), TNM stage(I + II vs. III; $P = 0.017$) , and high LRRC15 protein levels (high vs. low; $P < 0.01$) were adverse predictors of survival in TNBC patients. Multivariate Cox proportional hazards analysis confirmed that high LRRC15 protein levels (high vs. low; $P = 0.007$) were an independent prognostic factor for PFS (Table 2). In summary, our findings collectively suggest that LRRC15 is upregulated in TNBC tissues and cells and is associated with an unfavourable prognosis in patients with TNBC.

The overexpression of LRRC15 in TNBC suggests a pivotal role for LRRC15 in TNBC tumorigenesis

Next, we conducted knockdown and overexpression studies in the MDA-MB-231 and BT-549 cell lines, which exhibit moderate LRRC15 expression. WB assays were used to evaluate the efficiency of plasmid-mediated overexpression and small interfering RNA (siRNA)-mediated knockdown in these cell lines. The results demonstrated that LRRC15 expression in the siLRRC15-1 and siLRRC15-2 groups was consistently and significantly decreased (Fig. 2A). Conversely, LRRC15 expression was markedly elevated in the experimental group following overexpression plasmid transfection compared with the control group (Fig. 2B). The proliferation of MDA-MB-231 and BT-549 cells was significantly impaired by LRRC15 knockdown, as assessed by CCK-8 and colony formation assays. In contrast, LRRC15 overexpression significantly increased cell proliferation (Fig. 2C, D). To elucidate the mechanisms underlying the growth effects of LRRC15 knockdown on the inhibition of , we utilized flow cytometry to examine the impact of LRRC15 knockdown on cell cycle progression and apoptosis. We observed a significant increase in apoptosis in MDA-MB-231 and BT-549 cells treated with siLRRC15-1 or siLRRC15-2, whereas apoptosis was markedly reduced in cells overexpressing LRRC15 (Fig. 3A). Our results indicated that LRRC15 knockdown increased the proportion of cells in the G1 phase, consequently decreasing the proportion of cells entering the S phase, suggesting that LRRC15 knockdown induced G1–S cell cycle arrest in TNBC cells ($P < 0.05$). In contrast, LRRC15 overexpression facilitated TNBC cell cycle progression (Fig. 3B). Collectively, these findings demonstrate that LRRC15 knockdown inhibits TNBC cell growth by inducing G1–S phase cell cycle arrest and promoting apoptosis.

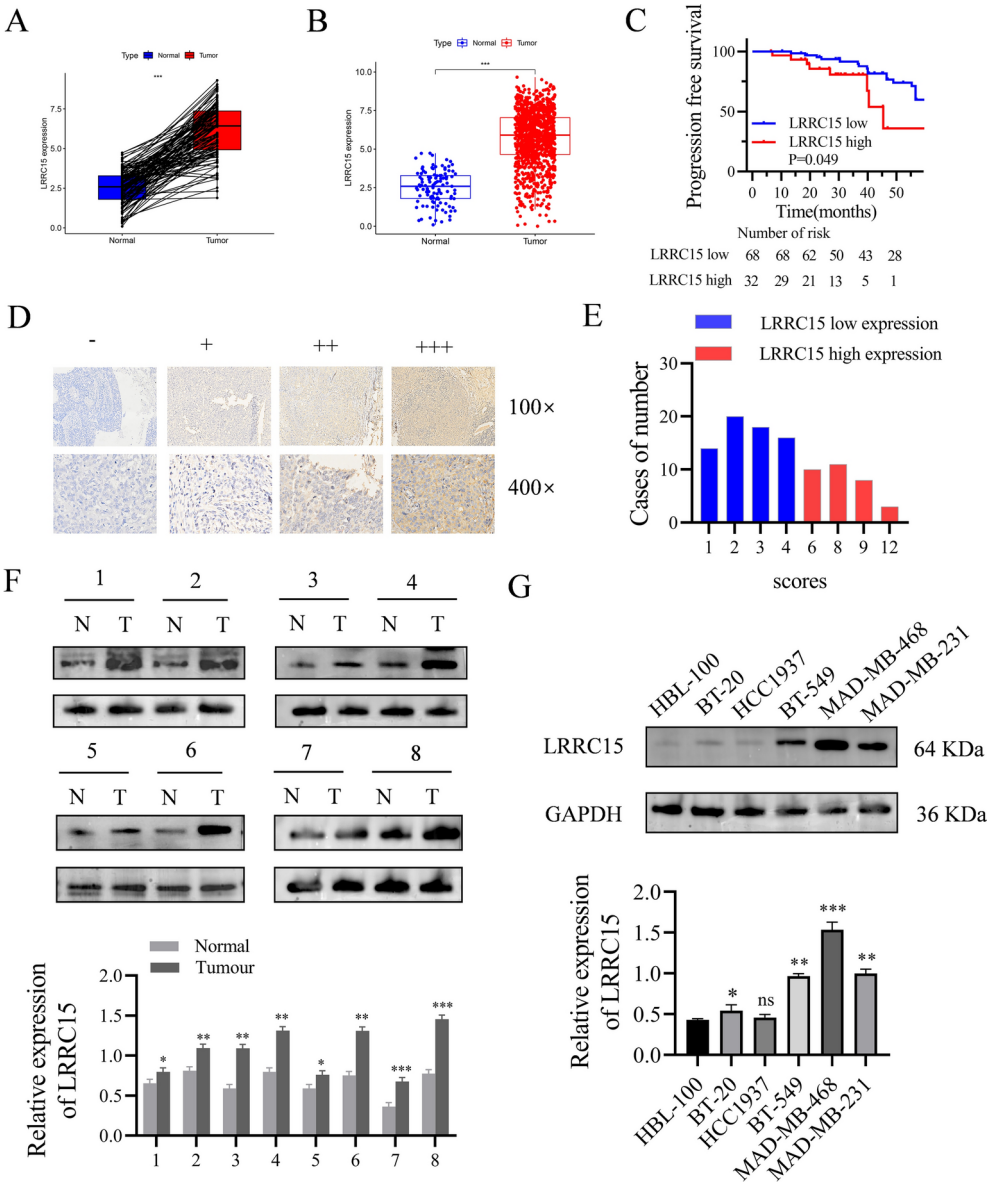

Fig. 1. LRRC15 is highly expressed in TNBC tissues and cells. (**A**) Paired difference analysis and (**B**) unpaired difference analysis of LRRC15 expression in tumor tissues and paraneoplastic tissues of TNBC patients in TCGA database. (**C**) Kaplan-Meier analysis of the correlation between LRRC15 and the progression free survival of TNBC patients. (**D**) Representative images of LRRC15 IHC expression in both tumor and normal tissues with varying levels. Original magnification, ×100, ×400. (**E**) TNBC tissues stratified by the IHC staining index. (**F**) Western blot analysis of LRRC15 protein expression levels in fresh TNBC tissue compared with para-cancerous tissue. (**G**) LRRC15 protein levels in different TNBC cell lines as assessed by WB. *p < 0.05; **p < 0.01; ***p < 0.001.

LRRC15 knockdown inhibits the migration and invasion of TNBC cells in vitro

We investigated the role of LRRC15 in TNBC cell motility using both wound healing and Transwell assays. These assays provided clear evidence that the knockdown of LRRC15 in MDA-MB-231 and BT-549 cells led to a substantial reduction in their migratory capacity compared with that of the control group. Conversely, the overexpression of LRRC15 resulted in increased migratory ability in these cells, surpassing that of the control group (Fig. 4A). Additionally, the Transwell Matrigel invasion assay revealed that the knockdown of LRRC15 significantly decreased the invasive potential of MDA-MB-231 and BT-549 cells. In stark contrast, the overexpression of LRRC15 increased their invasive capacity (Fig. 4B). These findings underscore the pivotal role of LRRC15 in modulating the metastatic properties of TNBC cells, suggesting that LRRC15 may serve as a key facilitator of cell migration and invasion. The manipulation of LRRC15 levels, therefore, presents a potential therapeutic strategy for impeding the metastatic spread of TNBC.

Clinicopathologic feature	Number	Low expression, N (%)	High expression, N (%)	P value
Age				
≤50	52	33 (63.46)	19 (36.54)	
> 50	48	35 (72.82)	13 (27.08)	0.311
Menopausal				
Yes	52	32 (61.54)	20 (38.46)	
No	48	36 (75.00)	12 (25.00)	0.149
Number of primary tumours				
1	90	62 (68.89)	28 (31.11)	
> 1	10	6 (60.00)	4 (40.00)	0.568
Lymphatic metastasis				
No	54	43 (79.63)	11 (20.37)	
Yes	46	25 (54.35)	21 (45.65)	**0.007**
Histological grade				
I	11	9 (81.82)	2 (18.18)	
II	81	52 (64.20)	29 (35.80)	
III	8	7 (87.50)	1 (12.50)	0.234
International TNM staging				
Stage I	12	12 (100.00)	0 (0.00)	
Stage II	81	49 (60.49)	31 (38.27)	
Stage III	7	7 (100.00)	0 (0.00)	**0.004**
Ki-67				
≤30	46	40 (86.96)	6 (13.04)	
> 30	54	28 (51.85)	26 (48.15)	<**0.001**
P53				
-/+	60	42 (70)	18 (30)	
++/+++	40	26 (65)	14 (35)	0.6
Neoadjuvant chemotherapy				
Yes	23	13 (56.52)	10 (43.48)	
No	77	36 (46.75)	41 (53.25)	0.305

Table 1. The basic information of 100 patients with TNBC.

Characteristic	Univariate analysis			Multivariate analysis		
	HR	95%CI	P value	HR	95%CI	P value
Age	1.109	0.671-1.834	0.686			
Menopausal state	0.973	0.588-1.610	0.916			
Number of primary tumours	1.351	0.614-2.976	0.455			
Lymph node metastasis	1.921	1.150-3.209	0.013	1.636	0.857-3.55	0.364
Histological grade	1.007	0.586-1.733	0.979			
TNM stage	2.035	1.134-3.652	0.017	1.744	0.857-3.550	0.125
Ki-67	1.641	0.987-2.729	0.056	0.808	0.294-2.224	0.68
P53	1.267	0.761-2.110	0.363			
Neoadjuvant chemotherapy	1.884	1.130-3.141	0.475			
LRRC15 expression	2.493	1.455-4.273	<0.01	2.231	1.251-3.978	**0.007**

Table 2. Univariate and multivariate Cox regression analysis of progression free survival in 100 TNBC patients. *CI* confidence interval, *HR* hazard ratio.

LRRC15 knockdown suppresses the growth of TNBC cell carcinoma in nude mice

To assess the impact of LRRC15 on tumour growth in vivo, we established stable LRRC15-knockdown strains using lentiviral-mediated gene silencing. WB was utilized to confirm the efficiency of LRRC15 knockdown, and the sh-Lrrc15#1 strain was selected for further investigation (Fig. 5A). We then developed a subcutaneous xenograft mouse model by injecting stably transfected sh-Lrrc15#1 or sh-Ctrl 4T1 cells into nude mice. Bioluminescence imaging of the subcutaneous tumours further demonstrated that the sh-Lrrc15#1 group exhibited a markedly lower total fluorescence intensity than the sh-Ctrl group did, indicating a reduced tumour burden (Fig. 5B). Comparative images of tumour formation in these mice revealed a noticeable reduction in tumorigenesis in

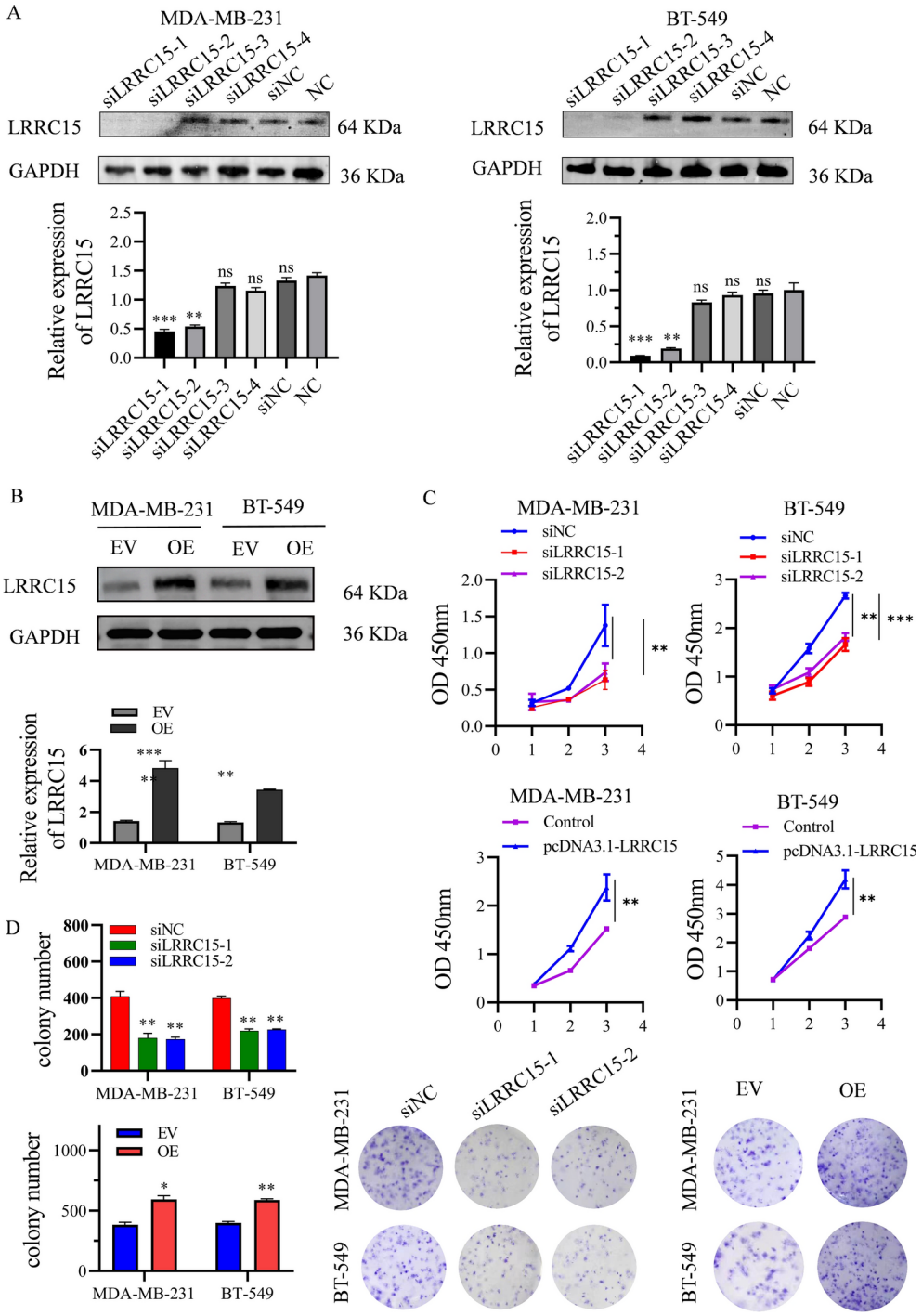

Fig. 2. LRRC15 promotes TNBC cell growth in vitro. (**A**,**B**) The transfection efficiency of the LRRC15 small interference and overexpression plasmi was confirmed by WB. (**C**) The effect of LRRC15 knockdown and overexpression on the proliferation of MDA-MB-231 and BT-549 cells was assessed by the CCK-8 assay. (**D**) The proliferation ability of LRRC15 cells after knockdown and overexpression was determined by clonal formation assay. *p < 0.05; **p < 0.01; ***p < 0.001.

the LRRC15-knockdown group compared with the control group (Fig. 5C). Quantitative analysis confirmed that both tumour volume and weight were significantly lower in the sh-Lrrc15#1 group than the sh-Ctrl group ($P < 0.001$) (Fig. 5D, E). Immunohistochemical analysis was performed to evaluate the expression of Ki-67, a proliferation marker, as well as MMP2 and MMP9, which are associated with metastasis. Consistent with our in vitro data, the sh-Lrrc15#1 group presented significantly lower expression of these markers than the sh-Ctrl group did (Fig. 5F). These in vivo findings corroborate our in vitro results, collectively suggesting that LRRC15

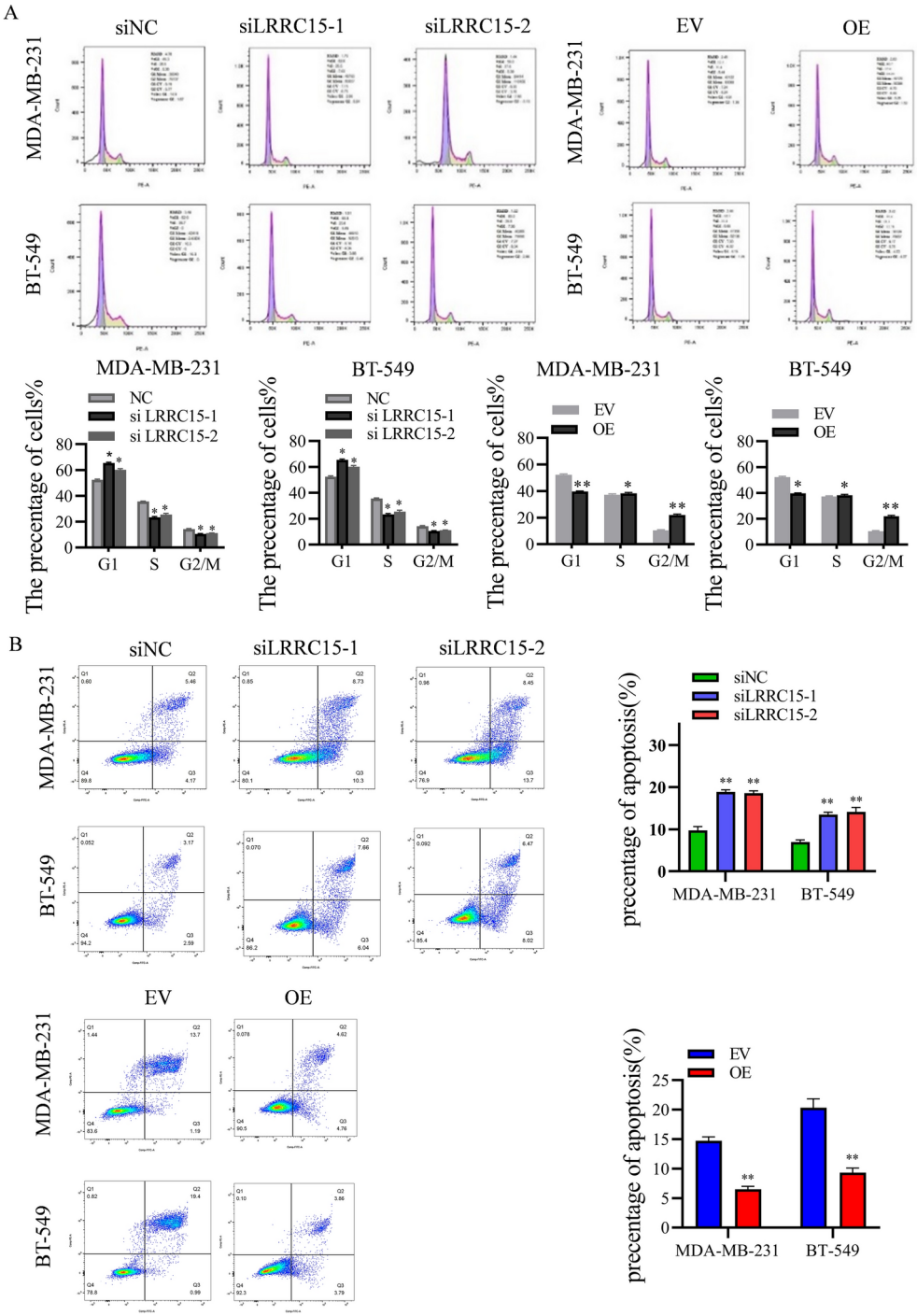

Fig. 3. The effects of LRRC15 on cell cycle and apoptosis of TNBC cells in vitro. (**A**) Flow cytometry was performed to analyze the distribution of the cell cycle in MDA-MB-231 and BT-549 cells subjected to LRRC15 overexpression or knockdown. (**B**) Flow cytometry was performed to analyze the distribution of the apoptosis in MDA-MB-231 and BT-549 cells subjected to LRRC15 overexpression or knockdown. *p < 0.05; **p < 0.01; ***p < 0.001.

knockdown can effectively suppress the proliferation, invasion, and migration of TNBC cells both in vivo and in vitro.

LRRC15 enhances TNBC proliferation, invasion, and migration by regulating the ITGB1/FAK/PI3K pathway

In this study, we performed whole transcriptome RNA sequencing to investigate the potential downstream regulatory units of LRRC15. Compared with the siNC group, the siLRRC15 group exhibited 449 significantly

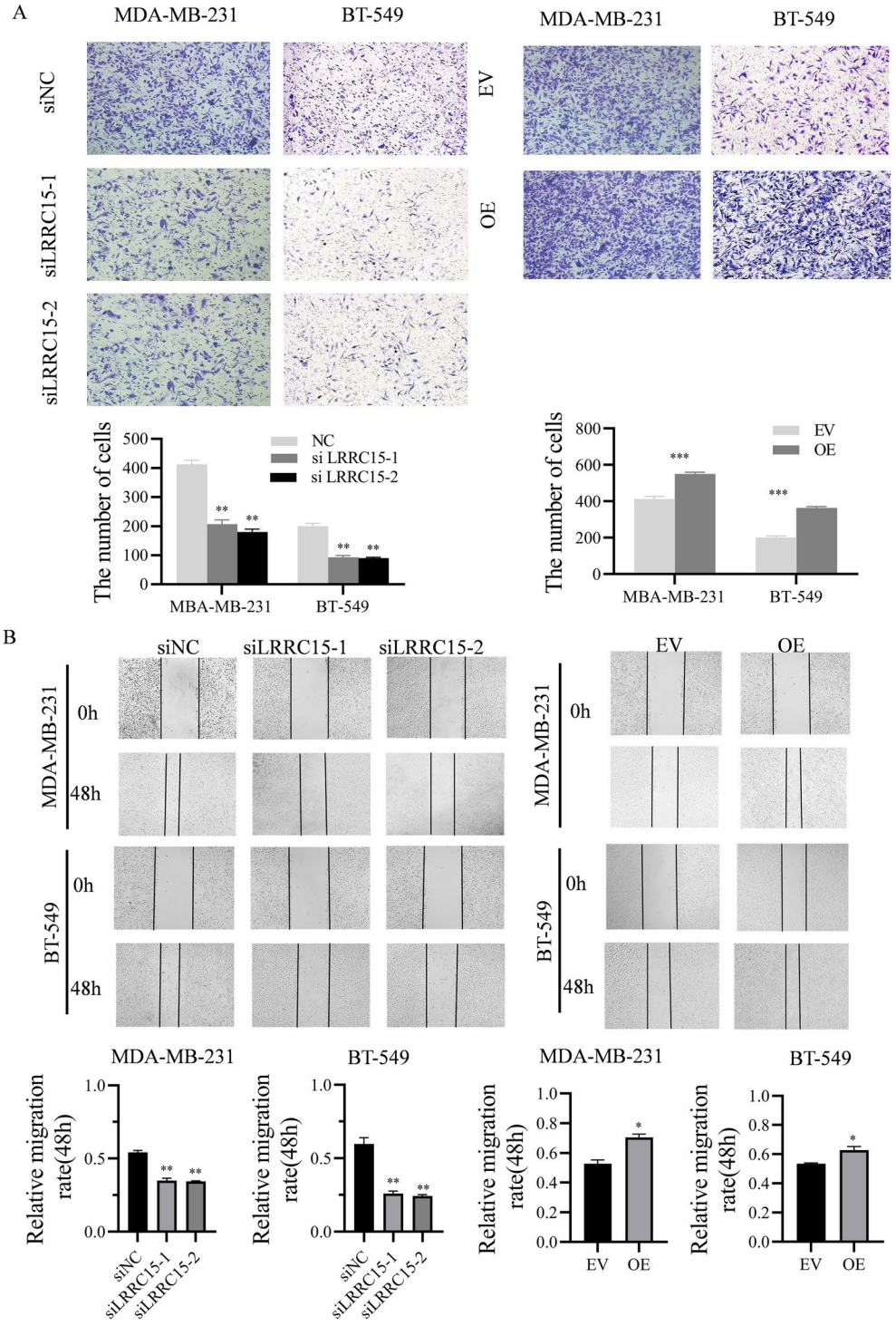

Fig. 4. The effects of LRRC15 on migration, invasion abilities of TNBC cells in vitro. (**A**) The Transwell experiment evaluated the alterations in the invasion capability of TNBC cells after the knockdown and overexpression of LRRC15. (**B**) The wound-healing assay results demonstrate the migration capabilities of MD-MB-231 and BT-549 cells in the siNC/siLRRC15-1/siLRRC15-2 and EV/OE groups. *p < 0.05; **p < 0.01; ***p < 0.001.

downregulated mRNAs and 508 significantly downregulated mRNAs. These findings clearly indicate that there are numerous regulatory factors downstream of LRRC15, highlighting the extensive and significant role of LRRC15 in TNBC. GO analysis revealed that cell proliferation, intercellular connectivity, and immune system processes significantly changed following the downregulation of LRRC15 expression. Kyoto Encyclopedia of Genes and Genomes (KEGG)[18] analysis revealed that differentially expressed genes were predominantly

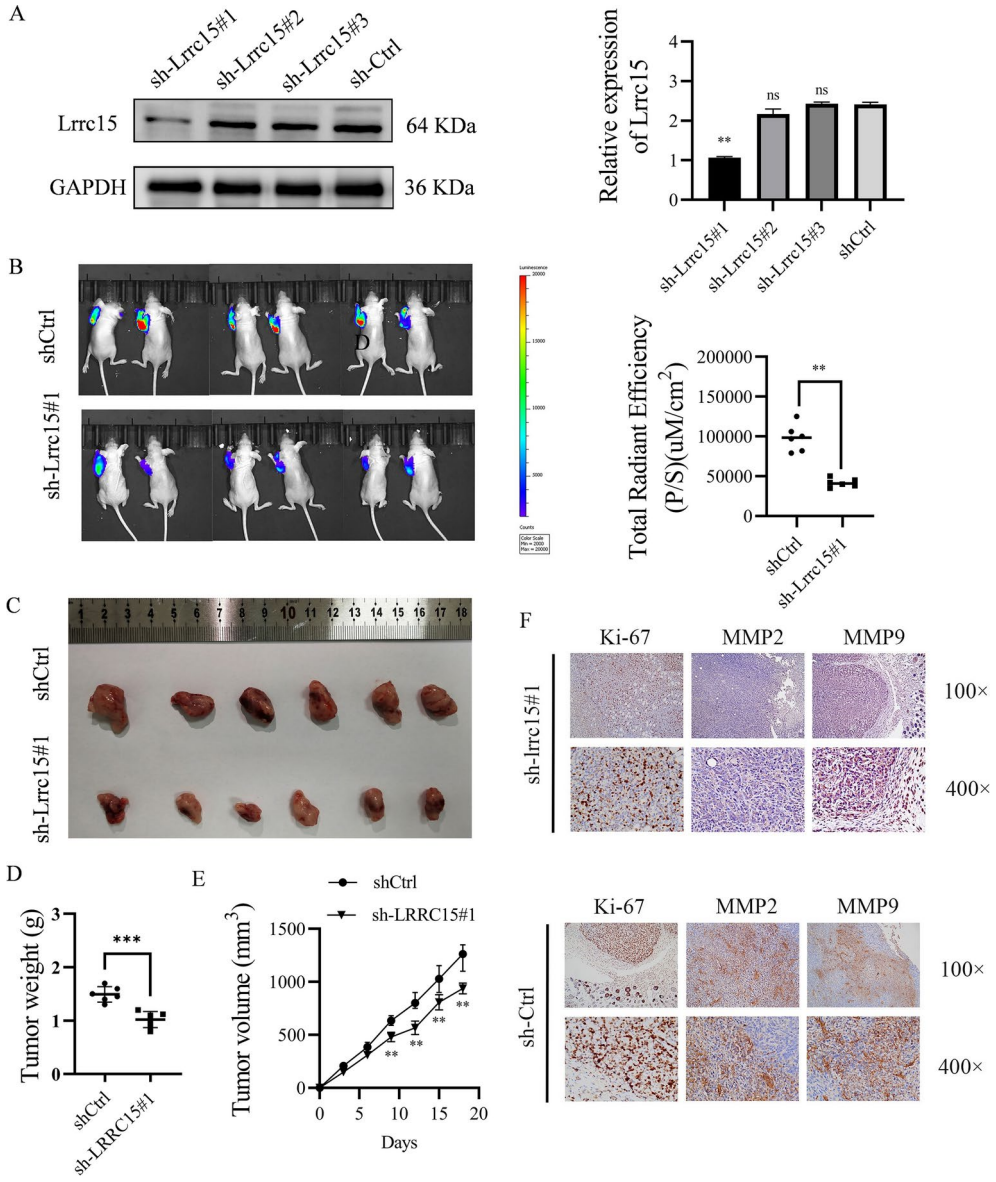

Fig. 5. Knockdown of LRRC15 significantly inhibits subcutaneous tumour growth in nude mice (n = 6). (**A**) After transfecting 4T1 cells with a lentivirus, the efficiency of knockdown was evaluated using Western blotting. (**B**) Representative bioluminescent images and quantification of signal intensities from bioluminescent imaging in nude mice for shCtrl and sh-Lrrc15#1 groups. (**C**) Representative image of subcutaneous tumours from nude mice in the shCtrl and sh-Lrrc15#1 groups. (**D**,**E**) Tumour weight and volume in the shCtrl and sh-Lrrc15#1 groups. (**F**) Immunohistochemical examination showed the expression of Ki-67, MMP2 and MMP9 in shCtrl and sh-Lrrc15#1 groups. *p < 0.05; **p < 0.01; ***p < 0.001.

enriched in the PI3K/AKT signalling pathway, focal adhesion pathway, and cytokine–cytokine interaction pathway . Further, KEGG enrichment analysis was performed on the genes differentially expressed by LRRC15 in the high-low-expression group of TNBC patients from the TCGA database using bioinformatics methods[19]. The results indicated that the differentially expressed genes were enriched primarily in the PI3K/AKT signalling pathway, focal adhesion, and extracellular matrix receptor interactions. The results of the KEGG enrichment analysis suggest that the PI3K/AKT signalling pathway and focal adhesion may serve as the primary regulatory units downstream of LRRC15. The autophosphorylation of FAK at Y397 serves as the binding site for PI3K[20]. As PI3K/AKT is a downstream molecule of FAK, activated PI3K/AKT signalling events are crucial for regulating cell viability and migration. Further detection via WB indicated that after LRRC15 was knocked down, the levels of the related proteins p-ITGB1 (T788/T789)/ITGB1, p-FAK (Tyr397)/FAK, p-PI3K (Tyr458)/PI3K and p-AKT(Ser473)/AKT were significantly reduced (Fig. 6A). These findings suggest that the activation of the ITGB1/FAK/PI3K pathway is inhibited.

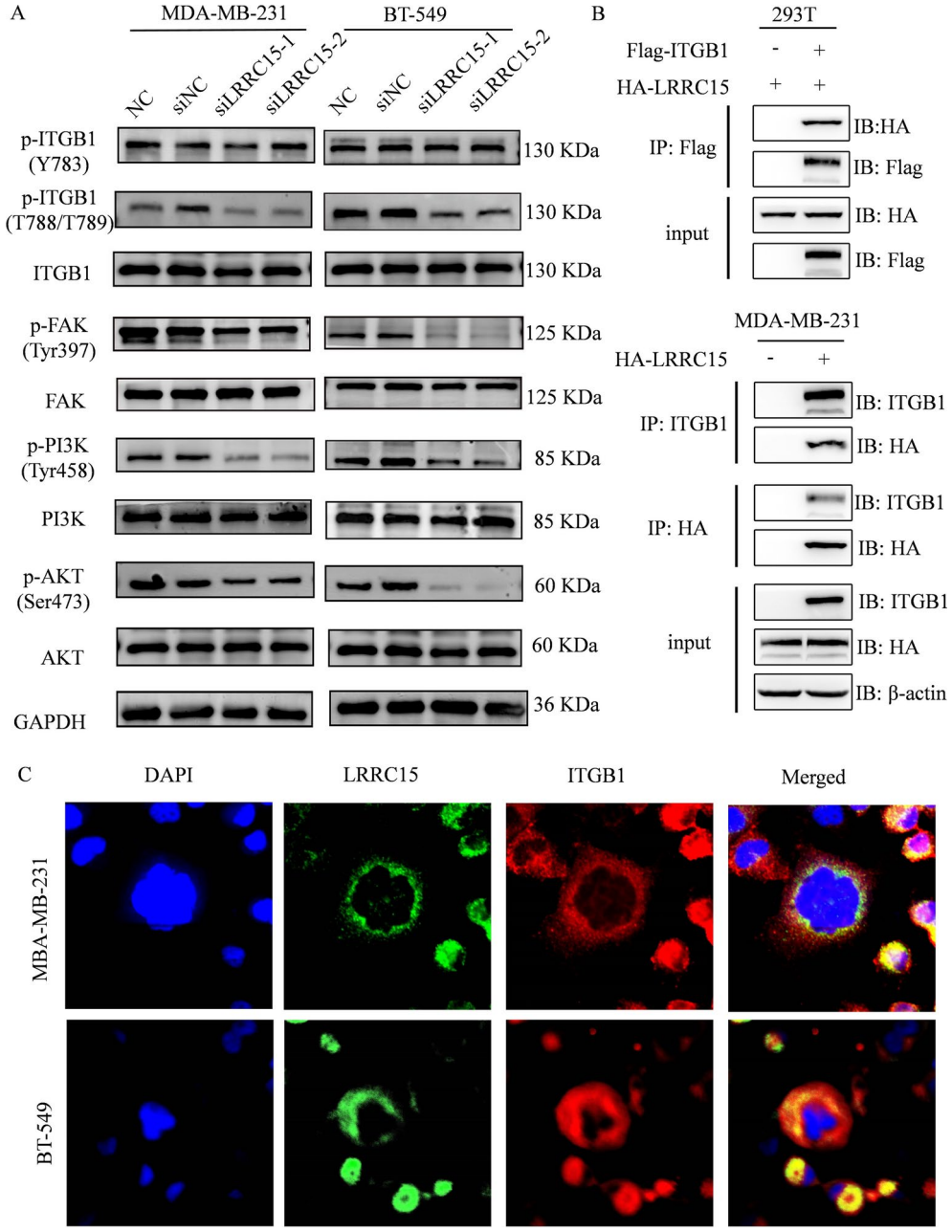

Fig. 6. WB analysis of ITGB1/FAK/PI3K signalling pathway protein expression in MBA-MB-231 and BT-549 cells with LRRC15 knockdown. (**A**) The expression of p-ITGB1, ITGB1, p-FAK, FAK, p-PI3K, PI3K, p-AKT, AKT protein was detected by WB. (**B**) Co-localization of LRRC15 (green) and ITGB1 (red) in MDA-MB-231 and BT-549 cells via immunofluorescence cytochemical analysis. The nucleus was stained with DAPI. Original magnification: ×100. (**C**) CoIP detects the interaction between LRRC15 and ITGB1. *P < 0.05; **p < 0.01; ***p < 0.001.

LRRC15 activates ITGB1 via T788/T789 phosphorylation to drive TNBC progression

To delineate the functional interplay between LRRC15 and ITGB1 in TNBC, we first investigated whether the LRRC15-mediated oncogenic effects depend on ITGB1 activation. Immunoprecipitation assays in MDA-MB-231 and HEK293T cells confirmed a direct physical interaction between LRRC15 and ITGB1 (Fig. 6B), while immunofluorescence revealed their colocalization at the plasma membrane in TNBC cells (Fig. 6C). We hypothesized that LRRC15 binding induces ITGB1 activation via phosphorylation at the conserved T788/T789 residues. To test this hypothesis, we transfected TNBC cells (MDA-MB-231 and BT-549) with wild-type ITGB1 (ITGB1-wt) or a phosphorylation-deficient mutant (ITGB1-mut, T788A/T789A). Compared with those in the ITGB1-wt group, cells overexpressing the ITGB1-mut mutant exhibited significantly reduced phosphorylation levels of ITGB1 (T788/T789), FAK (Tyr 397), and PI3K (Tyr458) ($p < 0.01$). Notably, LRRC15 knockdown substantially attenuated the phosphorylation of these signalling components (ITGB1 T788/T789, FAK Tyr 397,

and PI3K Tyr458) in ITGB1-wt-expressing cells ($p < 0.01$). However, this suppressive effect was completely abrogated in ITGB1-mut-expressing cells, where no significant reduction in phosphorylation was observed for any of these targets ($p > 0.05$) (Fig. 7A). CCK-8 and colony formation assays revealed that, compared with ITGB1-wt control cells, ITGB1-mut-expressing cells exhibited markedly impaired proliferation ($p < 0.01$), with

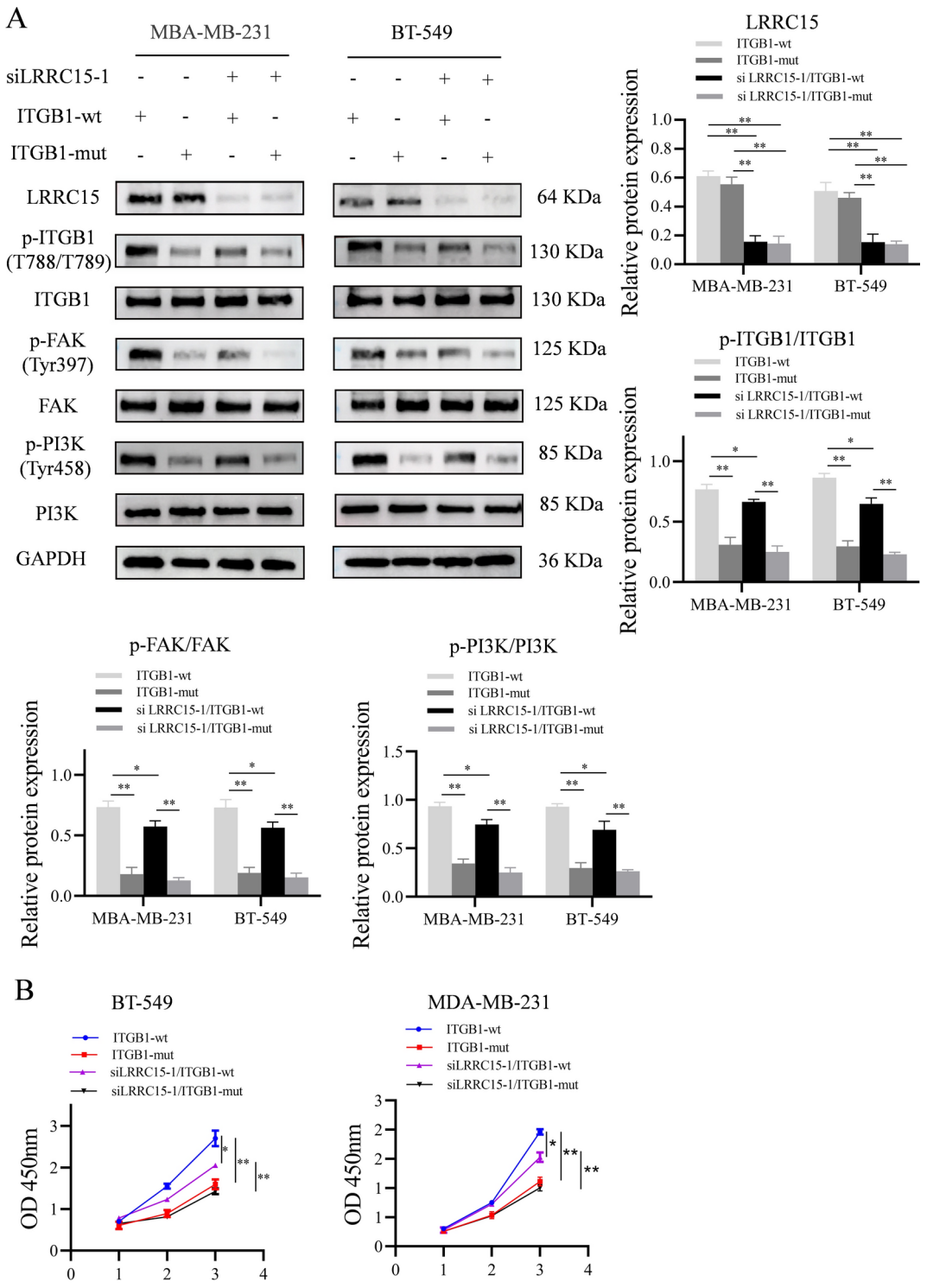

Fig. 7. LRRC15 promotes the growth and migration of TNBC cells dependent in part on phosphorylated T788/T789 sites of ITGB1. (**A**) WB method was used to verify the changes of ITGB1-wt or ITGB1-mut overexpression on ITGB1/FAK/PI3K signaling pathway after LRRC15 knockdown. (**B**) ITGB1-mut-expressing cells display significantly impaired proliferation compared to ITGB1-wt controls ($p < 0.01$). LRRC15 knockdown further suppresses growth in ITGB1-wt cells ($p < 0.01$) but fails to exert an additive inhibitory effect in ITGB1-mut-expressing cells ($p > 0.05$).

LRRC15 knockdown further suppressing the growth of WT cells ($p < 0.01$) but having no additive effect on MUT cells ($p > 0.05$) (Fig. 7B, 8A). Invasion and migration assays revealed decreased metastatic potential in MUT cells compared with WT cells. LRRC15 knockdown attenuated invasion in WT cells ($p < 0.01$), whereas the invasion of MUT-expressing cells remained refractory to this inhibition (Fig. 8B). Collectively, these data establish that LRRC15 binds ITGB1, induces T788/T789 phosphorylation, and activates downstream FAK/PI3K/AKT signalling to drive TNBC proliferation and migration. Disruption of this axis via LRRC15 knockdown or ITGB1-mut expression phenocopies the suppression of oncogenic traits, underscoring the centrality of the pathway in TNBC progression.

Discussion

TNBC represents approximately 15% of all breast cancers and is associated with a shorter overall survival time than other breast cancer types[21]. It is characterized by aggressive tumour behaviour, internal heterogeneity, and a lack of effective biomarkers, which contribute to treatment resistance, disease recurrence, and a poor prognosis[22]. Our study identified LRRC15 as a novel oncogenic driver in TNBC, bridging its clinical relevance to mechanistic insights into tumour progression.

LRRC15 located on chromosome 3q29, is a type I transmembrane protein comprising six domains: a signalling peptide, the characteristic LRR N-terminal domain, 15 LRRs, a C-terminal domain, a transmembrane domain, and a short cytoplasmic domain[23]. LRRC15 plays a pivotal role in mediating cell-cell and cell-extracellular matrix (ECM) interactions, including adhesion and receptor-ligand binding[24]. In cancer-associated fibroblasts, LRRC15 has been reported to promote the migration and invasion of TNBC cells by regulating them via the Wnt/β-catenin signalling pathway[25]. LRRC15 also promotes ovarian metastases, and LRRC15 antibody–drug

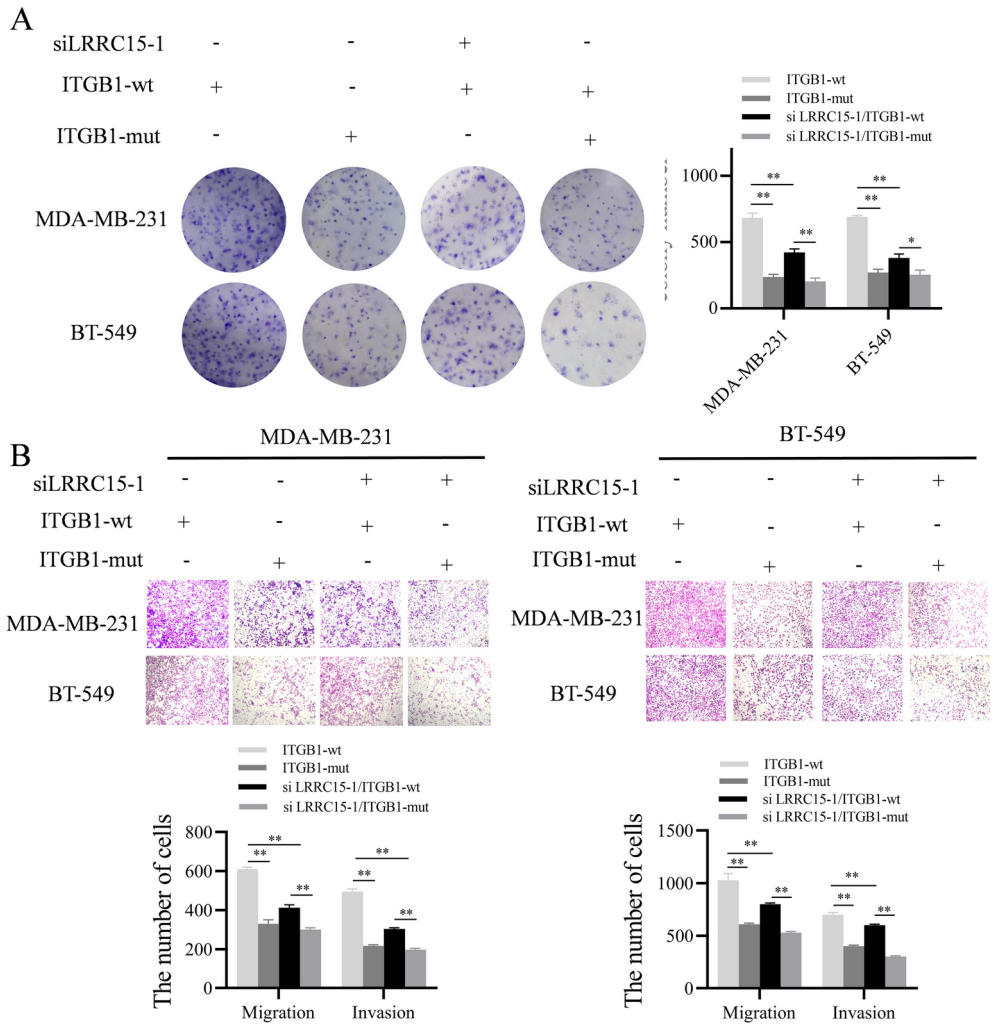

Fig. 8. (**A**) Colony-forming capacity is markedly reduced in ITGB1-mut-expressing cells relative to ITGB1-wt controls ($p < 0.01$). LRRC15 knockdown attenuates colony formation in ITGB1-wt cells ($p < 0.01$) but shows no significant suppression in ITGB1-mut-expressing cells ($p > 0.05$) (**B**) ITGB1-mut-expressing cells exhibit decreased invasive and migration potential compared to ITGB1-wt cells. LRRC15 knockdown significantly reduces invasion in ITGB1-wt cells ($p < 0.01$) but fails to inhibit invasive and migration in ITGB1-mut-expressing cells ($p > 0.05$).

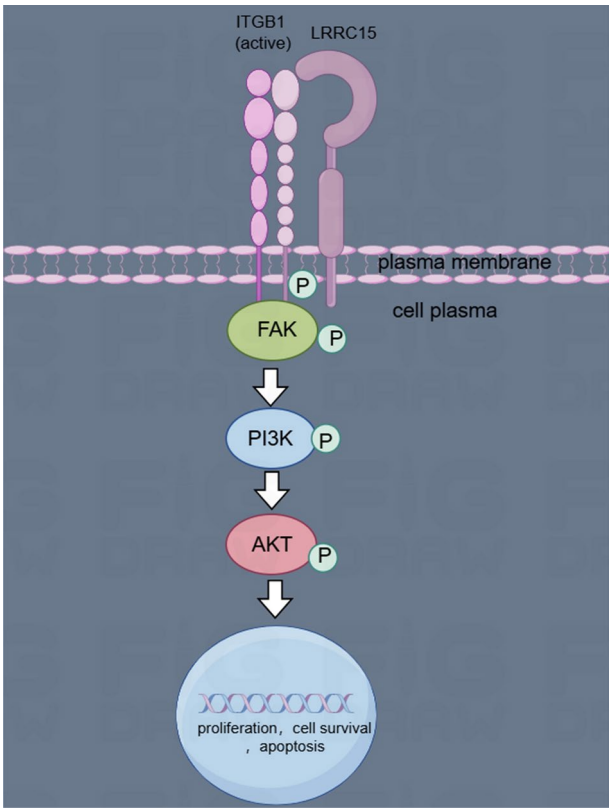

Fig. 9. Diagram of the mechanism of the LRRC15 gene in TNBC.

conjugates, such as ABBV-085, block intestinal and omental metastases in ovarian cancer[26]. While accumulating evidence suggests that LRRC15 could serve as a therapeutic target[16,27], its specific role in TNBC remains to be fully elucidated.

While prior studies have implicated LRRC15 in stromal remodelling and cancer-associated fibroblast regulation in other malignancies, our work uniquely establishes its cell-autonomous oncogenic role in TNBC. Mechanistically, LRRC15 directly interacts with integrin $\beta 1$ (ITGB1), a critical mediator of ECM-initiated signalling. This interaction stabilizes the phosphorylation of ITGB1 at the conserved T788/T789 residues. Phosphorylated ITGB1 recruits focal adhesion kinase (FAK) to integrin clusters, initiating downstream PI3K/AKT signalling (Fig. 9). Rescue experiments confirmed that LRRC15 knockdown suppresses PI3K/AKT activation and TNBC cell proliferation, whereas ITGB1 phosphorylation-deficient mutants (T788A/T789A) abrogate this effect, underscoring the dependency of the protumorigenic function of LRRC15 on ITGB1 activation. We found that LRRC15 expression was significantly elevated in TNBC tissues and cells and was an independent predictor of progression-free survival (PFS) (Table 2).

Integrins are pivotal in transducing extracellular signals and initiating downstream gene expression changes that regulate cellular adhesion, invasion, and migration[28]. Numerous integrins have been shown to be overexpressed in various cancer cell types, promoting tumour cell invasion and metastasis by binding to their ECM protein ligands[29]. Among them, integrin $\beta 1$ (ITGB1) interacts with specific ECM proteins, such as fibronectin (FN), collagen, and laminin, thereby activating multiple signalling pathways, including the FAK and PI3K pathways, which are instrumental in cell adhesion, invasion, and metastasis across different cancer types[30,31]. Phosphorylation of the conserved threonine motif (T788/T789) within the ITGB1 domain enhances integrin activity[32]. The TGB1 gene encodes $\beta 1$ integrin, which is intricately linked with cell adhesion and signalling. The phosphorylated states of T788 and T789 are believed to act as active switches for integrins[33,34]. This study confirmed through immunofluorescence and coimmunoprecipitation (co-IP) experiments that LRRC15 can directly bind to ITGB1, transitioning ITGB1 from an inactive state to an activated state, resulting in the phosphorylation of T788/T789 sites in the intracellular segment of ITGB1.

The dysregulation of phosphorylation and dephosphorylation events is closely associated with oncogenesis and tumour progression[35]. The phosphorylation of FAK at Tyr397 on a protein containing the SH2 domain creates binding sites for tyrosine protein kinases such as SRC and PI3K[36–38]. Our findings align with those of prior reports indicating that ITGB1/FAK/PI3K signalling is involved in cancer metastasis but differ in the identification of LRRC15 as a TNBC-specific upstream regulator. Unlike studies focusing on FAK autophosphorylation at Tyr397[39,40], we demonstrated that LRRC15 governs ITGB1 activation at T788/T789, a nodal point for integrin-mediated signalling. This upstream regulation provides a mechanistic rationale for the dual role of LRRC15 in promoting both proliferation (via PI3K/AKT-mediated cell cycle progression) and metastasis (through FAK-

dependent cytoskeletal remodelling). The clinical relevance of this pathway is further supported by reduced MMP2/MMP9 expression in LRRC15-depleted xenografts, which is consistent with impaired invasive capacity.

Despite these advances, our study has several limitations. First, while the role of LRRC15 in primary tumour growth was confirmed in subcutaneous xenografts, spontaneous metastasis models are needed to fully delineate its impact on TNBC dissemination. Second, the potential immunomodulatory role of LRRC15, as suggested by its stromal expression in other cancers, remains unexplored in TNBC. Finally, the therapeutic potential of LRRC15 inhibition warrants validation via the use of clinical-grade inhibitors or antibody–drug conjugates.

Our findings reveal an LRRC15-ITGB1-FAK-PI3K signalling axis that drives TNBC progression through phosphorylation-dependent mechanisms. The requirement for T788/T789 phosphorylation in mediating the oncogenic effects of LRRC15 suggests that targeting this interaction interface could achieve pathway-selective inhibition while sparing physiological integrin functions. As TNBC continues to evade current targeted therapies, LRRC15 shows promise as a target for therapeutic intervention and risk stratification.

Conclusion

LRRC15 was significantly expressed in TNBC cells and tissues and its level was negatively associated with patient survival outcomes. The interaction of LRRC15 with ITGB1 led to the phosphorylation of ITGB1 at T788 and T789, which in turn promoted the assembly of focal adhesion sites, enhancing TNBC cell proliferation and metastatic spread. These findings suggest that LRRC15 is a potential diagnostic biomarker and promising therapeutic target for TNBC intervention.

Methods

Cell lines and culture conditions

The TNBC cell lines MDA-MB-231, BT-549, BT-20, HCC1937, and MDA-MB-468 were procured from the cell bank of the Shanghai Institute of Biochemistry and Cell Biology, Chinese Academy of Sciences (Shanghai, China). The HBL-100 cell line was sourced from American Type Culture Collection (Manassas, VA, USA), and 4T1 cells were acquired from Suzhou Starfish Biotechnology (Suzhou, China). HBL-100 cells were cultured in McCoy's 5A medium (Gibco, Auckland, New Zealand), while MDA-MB-231 and MDA-MB-468 cell lines were cultured in Dulbecco's modified Eagle's medium (DMEM, Gibco, New Zealand). Other cell lines were grown in RPMI 1640 medium (Gibco, Grand Island, NY, USA). All media were supplemented with 10% fetal bovine serum (FBS; Gibco), $100U/ml$ penicillin, and $100\mu g/ml$ streptomycin. The cells were incubated at 37 $^{\circ}$C in a humidified 5% CO2 atmosphere. The authenticity of the human cell lines used in this study was ascertained through short tandem repeat (STR) profiling. Notably, all the experimental procedures were performed within the initial ten passages of each cell line, ensuring that the cells were free from mycoplasma contamination.

Lentivirus infection and siRNA transfection

LRRC15-specific siRNA (siLRRC15-1, siLRRC15-2), negative control siRNA (siNC), pcDNA3.1-LRRC15 (OE), empty vector (EV), pcDNA3.1-ITGB1, and LRRC15-targeting shRNA lentiviruses (sh-Lrrc15) were synthesized by GenePharma (Shanghai, China). ITGB1-wt and ITGB1-mut vectors were synthesized by Vigene Biosciences (Shandong, China). Transfections were performed with Lipofectamine 3000 (Invitrogen, Carlsbad, CA, USA) according to the manufacturer's protocol. The detailed sequence data can be found in Supplementary File 1: Excel S1. The knockdown and overexpression efficiencies were validated via Western blot (WB) analysis.

Patients and tissue samples

Formalin-fixed, paraffin-embedded (FFPE) tumour tissues from 100 TNBC patients who underwent surgery at the First Affiliated Hospital of Bengbu Medical College (2022-2023) were retrospectively analysed. The inclusion criteria were as follows: (1) histologically confirmed TNBC (ER/PR <1%, HER-2 IHC 0/1+ or ISH-negative); (2) TNM stages I-III; and (3) no neoadjuvant therapy. The exclusion criteria were as follows: (1) ambiguous diagnosis and (2) metastatic disease (stage IV). This study was approved by the Institutional Ethics Committee ([2022] No. 180).

Immunohistochemistry (IHC) and immunofluorescence (IF)

For IHC, Formalin Fixed Paraffin Embedded (FFPE) sections (4 μm) were deparaffinized, rehydrated, and subjected to antigen retrieval in citric acid buffer (pH 6.0, $95^{\circ}C$, 20 min). Endogenous peroxidase was blocked with 3% H2O2, followed by blocking with 5% goat serum. Primary antibodies against LRRC15 (Abcam, ab123456, 1:200), Ki-67 (Cell Signaling Technology, #9449, 1:400), MMP2 (#40994, 1:200), and MMP9 (#13667, 1:200) were incubated overnight at $4^{\circ}C$. The slides were developed with DAB (Dako, Glostrup, Denmark) and counterstained with haematoxylin. For IF, the cells were fixed with 4% paraformaldehyde, permeabilized with 0.1% Triton X-100, and incubated with an anti-LRRC15 antibody (1:100) followed by an Alexa Fluor 594-conjugated secondary antibody (Invitrogen, 1:500). Nuclei were stained with DAPI. Images were acquired using a Leica TCS SP8 confocal microscope (Leica Microsystems, Wetzlar, Germany).

Coimmunoprecipitation (Co-IP)

HEK293T or MDA-MB-231 cells transfected with pCDH-HA-LRRC15 or pCDH-FLAG-ITGB1 (System Biosciences) were lysed in IP buffer (25 mM Tris-HCl, pH 7.4; 150 mM NaCl; 1% NP-40; protease inhibitors). The lysates were incubated with anti-FLAG®M2 magnetic beads (Sigma–Aldrich, M8823) or HA-tag antibodies (Cell Signaling Technology, #3724) at $4^{\circ}C$ for 4 h. The beads were washed three times, and the bound proteins were eluted with 2× Laemmli buffer for WB analysis.

Cell counting Kit-8 (CCK8) assay

A CCK8 kit (Beyotime, Shanghai, China) was used to detect cell proliferation. Approximately 2×103 transfected cells/well were inoculated in 96-well plates and analysed at specified time points. Before detection,$10\mu L$ of CCK8 reagent was added to each well, the mixture was incubated at $37^{\circ}C$ for 1 h, and the absorbance at 450 nm was determined with a microplate reader.

Transwell assay

To conduct migration and invasion tests, cells were inoculated in serum-free medium within a Transwell (Corning, NY, USA) in the upper chamber ($8-\mu m$ pore size) or on a Matrigel-coated Transwell (Corning, NY, USA). The basal medium in the lower chamber contained $600\mu l$ of 10% foetal bovine serum as a chemical attractant. After incubation for 48 hours, the cells that had not migrated or invaded were gently removed from the upper chamber using a cotton swab. The remaining cells in the lower chamber were fixed with methanol, stained with 0.1% crystal violet for 15 minutes, and imaged using a microscope (Olympus Corporation, Tokyo, Japan). For each sample, five random fields of view (×100 magnification) were selected, and the cells in each field of view were counted.

Wound-healing assay

Transfected HCC cells (2×105cells per well) were inoculated into a six-well plate and cultured until they reached90% confluence. A $100\mu l$ plastic straw tip was then used to create a scratch in a single layer of cells, removing the displaced cells. The cells were subsequently supplemented with fresh medium containing a low serum concentration or no serum. Images were captured at 0 and 24 hours using an Olympus optical microscope. The relative migration of each group was measured using ImageJ software.

Western blot analysis

Total protein was extracted from the cells via RIPA buffer, supplemented with protease and phosphatase inhibitors, and the cells were boiled for 10 minutes. The protein concentration was determined using a BCA protein assay kit (Epizyme, Shanghai, China) following the manufacturer's instructions. A PowerPac HV High-Voltage Power Supply (Bio-Rad Laboratories, USA) was used for protein electrophoresis. The samples were then separated on a 10% or 12% sodium dodecyl sulfate (SDS)-polyacrylamide gel and transferred to a nitrocellulose membrane. Next, the membranes were blocked with 5% nonfat milk at room temperature for 2 hours. After being washed, they were incubated overnight at $4^{\circ}C$ with primary antibodies against LRRC15, p-ITGB1, ITGB1, p-FAK, FAK, p-SRC, SRC, p-PI3K,and PI3K, provided by Abcam (Cambridge, UK). The membranes were subsequently incubated with appropriate HRP-labelled secondary antibodies at room temperature for 2 hours. The bands were visualized using the ChemicDocXRS system (Bio-Rad, USA).

Flow cytometry analysis of the cell cycle and cell apoptosis

The cells were inoculated in 6-well culture plates and transfected with small interfering RNA 24 hours later. The cell cycle and apoptosis were assessed by flow cytometry 48 and 72 hours later. For cell cycle analysis, the cells were trypsinized, washed twice with cold PBS, and fixed overnight with cold 70% ethanol at $-20^{\circ}C$. The cells were washed with PBS twice and incubated with $10mg/ml$ RNase A, $400mg/ml$ propidium iodide, and 0.1% Triton X in PBS at room temperature for 30 minutes. The cells were then analysed by flow cytometry. Apoptosis was detected using an annexin V-FITC/PI apoptosis detection kit. The cells were collected and washed twice with cold PBS. They were then resuspended in $400\mu l$ of annexin binding buffer, supplemented with $5\mu l$ of annexin V-FITC and $10\mu l$ of PI, and incubated at room temperature for 25 minutes. Cell cycle progression and cell apoptosis were detected using flow cytometry (LSRFortessaTM X-20; BD Biosciences, San Jose, NJ, USA).

Xenograft mouse models

Twelve BALB/c nude mice (male, 6 weeks old) were purchased from Unilever (Beijing, China) and maintained under a 12 h light/12 h dark cycle with free access to food and water. The animals were reared in a laminar flow chamber in a laboratory at a room temperature of $27\pm2^{\circ}C$ and humidity of 40 to 60% without specific pathogens. To establish a subcutaneous xenograft model, 1×1064T1 cells stably infected with sh-Lrrc15#1 or shCtrl were injected subcutaneously into the flanks of each mouse. Tumour size was measured every three days. After 18 days, the tumours were excised and weighed. The volume was calculated using the formula: $volume = L \times W^2 \times 0.5$ (where L is the length and W is the width). The animal experiments were conducted in accordance with ARRIVE 2.0 guidelines (Animal Research: Reporting of In Vivo Experiments, https://arriveguidelines.org). Certificate number [2022] No. 274 was used for the animal experiments.

Bioinformatics analysis

RNA-seq data from the TCGA-TNBC cohort were retrieved via the GDC portal (https://portal.gdc.cancer.gov/). The raw counts were normalized using the DESeq2 package (v1.38.3) in R. Differential LRRC15 expression was assessed using the limma-voom pipeline ($|log2FC| \geq 1$, FDR-adjusted $p < 0.05$). The functional enrichment of the LRRC15-correlated genes (Pearson $|r| > 0.4$) was analysed via clusterProfiler (v4.8.1) using the Gene Ontology (GO) and Kyoto Encyclopedia of Genes and Genomes (KEGG) databases.

Statistical analysis

Statistical analyses were performed using SPSS 26.0 (IBM) and R software (version 4.3.1). The differential expression of LRRC15 across cancer types in the TCGA database was assessed using the Mann–Whitney U test (unpaired samples) or Wilcoxon signed-rank test (paired samples), with Benjamini–Hochberg correction for multiple comparisons ($FDR < 0.05$). Immunohistochemical scores (IRSs) were categorized into low

($IRS \leq 4$) and high ($IRS \geq 6$) expression groups, and clinicopathological correlations were evaluated using Pearson's chi-square test or Fisher's exact test for categorical variables. Survival outcomes were analysed using Kaplan-Meier curves with log-rank tests for univariate comparisons. The prognostic significance of the variables was further assessed by univariate and multivariate Cox proportional hazards regression models adjusted for covariates, including age, TNM stage, lymph node metastasis, and Ki-67 status. Hazard ratios (HRs) with 95% confidence intervals (CIs) are reported. Western blot and cell line expression data were analysed by Student's t test (two-group comparisons) or one-way ANOVA with Tukey's post hoc test (multiple groups). All the statistical tests were two-sided, and $P < 0.05$ was considered statistically significant. Graphical representations were generated using GraphPad Prism 9.0

Data availability

The datasets generated and/or analyzed during the current study are available in the NCBI BioProject repository under accession number PRJNA1191998 (https://www.ncbi.nlm.nih.gov/bioproject/PRJNA1191998). Publicly available datasets analyzed in this study, including TCGA-TNBC cohort data, were retrieved from the GDC portal (https://portal.gdc.cancer.gov/). Pathway analysis in this study utilized the Kyoto Encyclopedia of Genes and Genomes (KEGG) database (https://www.kegg.jp/). KEGG is a copyrighted resource under license from the Kanehisa Laboratories. The datasets generated during and/or analysed during the current study are available from the corresponding author on reasonable request.

Received: 14 November 2024; Accepted: 14 April 2025
Published online: 25 April 2025

References

1. Sung, H. et al. Global cancer statistics 2020: Globocan estimates of incidence and mortality worldwide for 36 cancers in 185 countries. *CA Cancer J. Clin.* **71**, 209–249. https://doi.org/10.3322/caac.21660 (2021).
2. Lehmann, B. D. et al. Multi-omics analysis identifies therapeutic vulnerabilities in triple-negative breast cancer subtypes. *Nat. Commun.* **12**, 6276. https://doi.org/10.1038/s41467-021-26502-6 (2021).
3. Dent, R. et al. Triple-negative breast cancer: Clinical features and patterns of recurrence. *Clin. Cancer Res.* **13**, 4429–4434. https://doi.org/10.1158/1078-0432.Ccr-06-3045 (2007).
4. Waks, A. G. & Winer, E. P. Breast cancer treatment: A review. *JAMA* **321**, 288–300. https://doi.org/10.1001/jama.2018.19323 (2019).
5. Perou, C. M. et al. Molecular portraits of human breast tumours. *Nature* **406**, 747–752. https://doi.org/10.1038/35021093 (2000).
6. Leon-Ferre, R. A. & Goetz, M. P. Advances in systemic therapies for triple negative breast cancer. *BMJ* **381**, e071674. https://doi.org/10.1136/bmj-2022-071674 (2023).
7. Yin, L., Duan, J. J., Bian, X. W. & Yu, S. C. Triple-negative breast cancer molecular subtyping and treatment progress. *Breast Cancer Res.* **22**, 61. https://doi.org/10.1186/s13058-020-01296-5 (2020).
8. Deepak, K. G. K. et al. Tumor microenvironment: Challenges and opportunities in targeting metastasis of triple negative breast cancer. *Pharmacol. Res.* **153**, 104683. https://doi.org/10.1016/j.phrs.2020.104683 (2020).
9. Derakhshan, F. & Reis-Filho, J. S. Pathogenesis of triple-negative breast cancer. *Annu. Rev. Pathol.* **17**, 181–204. https://doi.org/10.1146/annurev-pathol-042420-093238 (2022).
10. Ray, U. et al. Exploiting lrrc15 as a novel therapeutic target in cancer. *Can. Res.* **82**, 1675–1681. https://doi.org/10.1158/0008-5472.Can-21-3734 (2022).
11. Miron-Mendoza, M. et al. The role of vimentin in human corneal fibroblast spreading and myofibroblast transformation. *Cells* **13**, 1094. https://doi.org/10.3390/cells13131094 (2024).
12. Zhang, J. et al. Single-cell analysis reveals the col11a1(+) fibroblasts are cancer-specific fibroblasts that promote tumor progression. *Front. Pharmacol.* **14**, 1121586. https://doi.org/10.3389/fphar.2023.1121586 (2023).
13. Batsis, J. A. et al. Development and usability assessment of a connected resistance exercise band application for strength-monitoring. *World Acad. Sci. Eng. Technol.* **13**, 340–348. https://doi.org/10.5281/zenodo (2019).
14. Bierkens, M. et al. Focal aberrations indicate eya2 and hsa-mir-375 as oncogene and tumor suppressor in cervical carcinogenesis. *Genes Chromosomes Cancer* **52**, 56–68. https://doi.org/10.1002/gcc.22006 (2013).
15. Ben-Ami, E. et al. Lrrc15 targeting in soft-tissue sarcomas: Biological and clinical implications. *Cancers* https://doi.org/10.3390/cancers12030757 (2020).
16. Demetri, G. D. et al. First-in-human phase i study of abbv-085, an antibody-drug conjugate targeting lrrc15, in sarcomas and other advanced solid tumors. *Clin. Cancer Res.* **27**, 3556–3566. https://doi.org/10.1158/1078-0432.CCR-20-4513 (2021).
17. Krishnamurty, A. T. et al. Lrrc15(+) myofibroblasts dictate the stromal setpoint to suppress tumour immunity. *Nature* **611**, 148–154. https://doi.org/10.1038/s41586-022-05272-1 (2022).
18. Kanehisa, M. & Goto, S. Kegg: Kyoto encyclopedia of genes and genomes. *Nucleic Acids Res.* **28**, 27–30. https://doi.org/10.1093/nar/28.1.27 (2000).
19. Kanehisa, M. Toward understanding the origin and evolution of cellular organisms. *Protein Sci.* **28**, 1947–1951. https://doi.org/10.1002/pro.3715 (2019).
20. Kanehisa, M., Furumichi, M., Sato, Y., Kawashima, M. & Ishiguro-Watanabe, M. Kegg for taxonomy-based analysis of pathways and genomes. *Nucleic Acids Res.* **51**, D587–D592. https://doi.org/10.1093/nar/gkac963 (2023).
21. Collignon, J., Lousberg, L., Schroeder, H. & Jerusalem, G. Triple-negative breast cancer: Treatment challenges and solutions. *Breast Cancer Targets Ther.* **8**, 93–107. https://doi.org/10.2147/BCTT.S69488 (2016).
22. Obidiro, O., Battogtokh, G. & Akala, E. O. Triple negative breast cancer treatment options and limitations: Future outlook. *Pharmaceutics* https://doi.org/10.3390/pharmaceutics15071796 (2023).
23. O'Prey, J., Wilkinson, S. & Ryan, K. M. Tumor antigen lrrc15 impedes adenoviral infection: implications for virus-based cancer therapy. *J. Virol.* **82**, 5933–5939. https://doi.org/10.1128/JVI.02273-07 (2008).
24. Satoh, K., Hata, M. & Yokota, H. A novel member of the leucine-rich repeat superfamily induced in rat astrocytes by beta-amyloid. *Biochem. Biophys. Res. Commun.* **290**, 756–762. https://doi.org/10.1006/bbrc.2001.6272 (2002).
25. Yang, Y. et al. Cancer-associated fibroblast-derived lrrc15 promotes the migration and invasion of triple-negative breast cancer cells via wnt/beta-catenin signalling pathway regulation. *Mol. Med. Rep.* https://doi.org/10.3892/mmr.2021.12518 (2022).
26. Ray, U. et al. Targeting lrrc15 inhibits metastatic dissemination of ovarian cancer. *Can. Res.* **82**, 1038–1054. https://doi.org/10.1158/0008-5472.CAN-21-0622 (2022).
27. Hingorani, P. et al. Abbv-085, antibody-drug conjugate targeting lrrc15, is effective in osteosarcoma: A report by the pediatric preclinical testing consortium. *Mol. Cancer Ther.* **20**, 535–540. https://doi.org/10.1158/1535-7163.MCT-20-0406 (2021).

28. Kim, S. H., Turnbull, J. & Guimond, S. Extracellular matrix and cell signalling: the dynamic cooperation of integrin, proteoglycan and growth factor receptor. *J. Endocrinol.* **209**, 139–151. https://doi.org/10.1530/JOE-10-0377 (2011).
29. Hamidi, H. & Ivaska, J. Every step of the way: integrins in cancer progression and metastasis. *Nat. Rev. Cancer* **18**, 533–548. https://doi.org/10.1038/s41568-018-0038-z (2018).
30. Grzesiak, J. J. et al. Knockdown of the beta(1) integrin subunit reduces primary tumor growth and inhibits pancreatic cancer metastasis. *Int. J. Cancer* **129**, 2905–2915. https://doi.org/10.1002/ijc.25942 (2011).
31. Luo, J. et al. 14, 15-eet induces breast cancer cell emt and cisplatin resistance by up-regulating integrin alphavbeta3 and activating fak/pi3k/akt signaling. *J. Exp. Clin. Cancer Res.* **37**, 23. https://doi.org/10.1186/s13046-018-0694-6 (2018).
32. Grimm, T. M., Dierdorf, N. I., Betz, K., Paone, C. & Hauck, C. R. Ppm1f controls integrin activity via a conserved phospho-switch. *J. Cell Biol.* https://doi.org/10.1083/jcb.202001057 (2020).
33. Yu, Y. et al. Extracellular matrix stiffness regulates microvascular stability by controlling endothelial paracrine signaling to determine pericyte fate. *Arterioscler. Thromb. Vasc. Biol.* **43**, 1887–1899. https://doi.org/10.1161/ATVBAHA.123.319119 (2023).
34. Coopman, P. Protein phosphorylation in cancer: Unraveling the signaling pathways. *Biomolecules* https://doi.org/10.3390/biom12081036 (2022).
35. Hamadi, A. et al. Regulation of focal adhesion dynamics and disassembly by phosphorylation of fak at tyrosine 397. *J. Cell Sci.* **118**, 4415–4425. https://doi.org/10.1242/jcs.02565 (2005).
36. Chen, H. C. & Guan, J. L. Association of focal adhesion kinase with its potential substrate phosphatidylinositol 3-kinase. *Proc. Natl. Acad. Sci. U. S. A.* **91**, 10148–10152. https://doi.org/10.1073/pnas.91.21.10148 (1994).
37. Chen, H. C., Appeddu, P. A., Isoda, H. & Guan, J. L. Phosphorylation of tyrosine 397 in focal adhesion kinase is required for binding phosphatidylinositol 3-kinase. *J. Biol. Chem.* **271**, 26329–26334. https://doi.org/10.1074/jbc.271.42.26329 (1996).
38. Zhou, J., Jiang, Y. Y., Chen, H., Wu, Y. C. & Zhang, L. Tanshinone i attenuates the malignant biological properties of ovarian cancer by inducing apoptosis and autophagy via the inactivation of pi3k/akt/mtor pathway. *Cell Prolif.* **53**, e12739. https://doi.org/10.1111/cpr.12739 (2020).
39. Leng, Y. et al. Ppm1f regulates ovarian cancer progression by affecting the dephosphorylation of itgb1. *Clin. Transl. Oncol.* https://doi.org/10.1007/s12094-024-03614-1 (2024).
40. Wen, X., Hou, Y., Zhou, L. & Fang, X. Linc00969 inhibits proliferation with metastasis of breast cancer by regulating phosphorylation of pi3k/akt and ilp2 expression through hoxd8. *PeerJ* **11**, e16679. https://doi.org/10.7717/peerj.16679 (2023).

Acknowledgements

The authors gratefully acknowledge the data generated by TCGA databases used in this study.

Author contributions

Xiao Wu performed most of the experiments, Yongxia Chen and Zishu Wang analyzed data, Yameng Liu and Yinxi Hu contributed to experiments. Zhixiang Zhuang and Fang Su designed experiments, supervised the study, and wrote the manuscript.

Funding

This study was supported by Natural Science key project of Bengbu Medical College (No. 2021byzd064).

Declarations

Competing interests

The authors declare no competing interests.

Ethics approval

This study is performed in accordance with relevant guidelines and regulations. All animal use procedures were in accordance with the Guide for the Care and Use of Laboratory Animals (NIH publications no. 80-23, revised 1996) and were performed according to the institutional ethical guidelines for animal experiments. Certificate number [2022] No. 274 was used for the animal experiments. Animals were sacrificed using CO2 asphyxiation. This study was approved by the Ethics Committee of the First Affiliated Hospital of Bengbu Medical College [2022] No. 180. We confirmed that informed consent was obtained from all subjects and/or their legal guardian(s).

Additional information

Supplementary Information The online version contains supplementary material available at https://doi.org/10.1038/s41598-025-98661-1.

Correspondence and requests for materials should be addressed to Z.Z.